INTERNATIONAL JOURNAL OF INTEGRATED ENGINEERING
ISSN: 2229-838X e-ISSN: 2600-7916

IJIE

Vol. 16 No. 3 (2024) 28-35
https://publisher.uthm.edu.my/ojs/index.php/ijie

Investigation on Thermally Evaporated Aluminium Contact Layers for Perovskite Solar Cell Applications

Rachael Wan Lyn Sia[1], Pei-Ling Low[1]*, Abdelrahman Hamed Ebrahem Abdelhamed[1] , Gregory Soon How Thien[1], Yew-Keong Sin[1], Kah-Yoong Chan[1]

[1] *Centre for Advanced Devices and Systems, Faculty of Engineering, Multimedia University, Persiaran Multimedia, 63100 Cyberjaya, Selangor, MALAYSIA*

*Corresponding Author: pllow@mmu.edu.my
DOI: https://doi.org/10.30880/ijie.2024.16.03.003

Article Info

Received: 11 November 2023
Accepted: 2 January 2024
Available online: 29 April 2024

Keywords

Perovskite solar cell, aluminium thin film, metal contact layer, thermal evaporation

Abstract

Perovskite solar cells (PSCs) have gained wide interest due to their high device efficiency of up to 22.1%. Perovskite solar cells are comprised of five main layers: fluorine-doped tin oxide (FTO) glass, titanium dioxide (TiO2) electron transport layer (ETL), perovskite active layer, Spiro-OMeTAD hole transport layer (HTL), and a metal contact layer. The metal contact layer plays a significant role in collecting and transporting the generated current and hence governs the performance of the device. Aluminium (Al) is more cost-efficient than the commonly used silver (Ag) or gold (Au) contact layers in perovskite solar cells. The aim of this work is to investigate the influence of different thicknesses and surface morphologies on the electrical properties of the Al thin film contact layers for perovskite solar cell applications. The Al contact layers were deposited using a thermal evaporator with varying Al wire source lengths at constant deposition duration and pressure. The deposited films were characterised for thickness, morphology, and electrical properties using a stylus profilometer, an atomic force microscope, and a four-point probe, respectively. Results showed that thicker Al films have larger particle sizes as compared to the thinner films, demonstrating a more continuous film morphology. Resistivity and conductivity show a variance with different film thickness. Based on literature, higher conductivity and larger particle sizes of the metal contact layers can improve charge transportation, which contributes to the performance of the perovskite solar cell.

1. Introduction

Perovskite solar cells (PSCs) have gained prominence due to their remarkable power conversion efficiencies, which have rapidly increased since 2009 from 3.8% to 22.1% [1] via ongoing research and development efforts. These efficiencies are comparable to those of the more commonly used silicon-based photovoltaic devices and have the potential to replace them on the market. The perovskite mineral has many unique properties that contribute to its exceptional performance. They possess a direct bandgap, meaning they can efficiently absorb a wide range of sunlight wavelengths, which can improve their sunlight conversion rate. The direct bandgap also makes it able to pair with lower bandgap photovoltaic technology [2]. Additionally, perovskites can be easily synthesised from low-cost and abundant materials, making them an attractive alternative to conventional solar cell materials. The fabrication of PSCs is relatively simple and can be performed using solution-based methods such as spin coating [3], printing [4], or vapour deposition [5].

The metal contact layer is a fundamental component in the fabrication of a solar cell, as it facilitates the efficient extraction and collection of photogenerated electrons and holes within the device by creating a pathway for the charge carriers that has low resistance. The importance of an efficient charge carrier is to ensure that the photogenerated charges are effectively utilised. To reduce recombination and resistive losses, the choice of metal, electrical conductivity, design of the layer, and its compatibility with the hole transport layer are critical to achieving a reliable and high-performance device. The use of aluminium (Al) metal as the back contact in a PSC is not as common as the use of gold (Au) and silver (Ag) metals. However, it is an attractive alternative due to its abundance and cost-effectiveness. The Al layer would be thermally deposited onto the hole transport layer (HTL), which is the Spiro-OMeTAD layer. Al metal has a relatively high electrical conductivity of 37.67 $mS \cdot m^{-1}$ [6] and a relatively low resistivity $2.7 \pm 0.1 \times 10^{-16}$ Ω·m, making it a good metal for transporting electrical current and reducing resistive current, thus causing it to be widely used in electrical and electronics applications. The objective of this work is to investigate the different thicknesses, morphologies, and topographies of the thermally deposited Al thin films in relation to their electrical properties for the application of the back contact for PSCs. The thickness of the Al thin films was manipulated by varying the length of the source Al wires. The resultant Al thin films were then characterized using a 4 -point probe and an atomic force microscope (AFM). The results found that Sample A demonstrated the most suitable parameters with a resistivity of 6.14 μΩ·m, and a conductivity of 162.86 $kS \cdot m^{-1}$.

The contents of this paper include a literature review in Section 2, detailing about perovskite solar cells, the metal contact layer, and comparisons of various metal contact materials. This is followed by the methodology in Section 3 which covers the aluminium thin film contact layer fabrication and the aluminium thin film measurement methods. In Section 4, the results and data presentation of the thickness, morphology, and electrical properties of the Al thin films are discussed. Finally, the findings in Section 4 are summarised and concluded in Section 5.

2. Literature Review

2.1 Perovskite Solar Cell

Perovskite solar cells (PSCs) are a type of photovoltaic technology that harnesses perovskite materials to convert sunlight into electricity. These solar cells are named after the crystal structure of the light-absorbing material, which resembles the naturally occurring mineral perovskite [7]. The key component of a PSC is the perovskite layer, which is typically made of a hybrid organic-inorganic material. The most commonly used perovskite material is methylammonium lead iodide ($CH_3NH_3PbI_3$) [8]. The device structure of a PSC is fundamentally made up of five layers: the transparent conducting oxide (TCO), electron transport layer (ETL), organic-metal halide perovskite layer, hole transport layer (HTL), and a metal top contact layer [9]. The process of generating electricity in a PSC starts when sunlight strikes the perovskite layer. The photons in the sunlight energise the electrons in the perovskite material, causing them to move and create electron-hole pairs. The excited electrons are then collected and transported away from the perovskite layer by an electron transport layer, while the holes are collected by a hole transport layer. The separated electrons and holes are funnelled towards their respective electrodes: an electron collection electrode and a hole collection electrode [10]. These electrodes enable the extraction of the electrical current generated by the movement of the charge carriers. Typically, a TCO, such as indium tin oxide (ITO) or fluorine tin oxide (FTO), is used as the bottom electrode to allow the sunlight to penetrate through to the electron transport layer and the perovskite layer. The top electrode is typically made of gold (Au), silver (Ag), carbon (C), or aluminium (Al) [11].

2.2 Metal Contact Layer

One of the important roles of the metal contact layer in a solar cell is to collect the generated charge carriers from the active layer and the hole transport layer. These charge carriers are then transported to the external circuit via the metal contact layer. An electrical current can go through the metal contact layer with little resistance. Due to their high conductivity and low resistance, metals are excellent for charge transfer from the solar cells to external circuits. As such, the type of metal used as the metal contact layer is important, as different metals have different electrical properties. The metals that are most commonly used in perovskite solar cells are gold (Au), silver (Ag), aluminium (Al), and carbon (C) for their low resistivity, high conductivity, and simple fabrication methods. Au, Ag, and Al metals can be fabricated via thermal evaporation [5], [12], [13], sputtering, and electron-beam evaporation [9], while C electrodes can be deposited via the doctor blade method [14].

2.3 Comparisons on Various Metal Contact Materials

As aforementioned, different metals will yield different properties. The methods of fabrication, thickness of the layer, and morphology contribute to the various parameters that can govern the resultant characteristics of the

Int. Journal of Integrated Engineering Vol. 16 No. 3 (2024) p. 28-35

thin film formed. As presented in Table 1, the different metal contact materials, fabrication methods, thickness, and grain size will contribute to differing electrical properties.

Table 1 *Comparisons on the parameters of various metal contact materials*

Metal	Fabrication Method	Thickness of Layer	Grain Size	Conductivity	Reference
Al	Thermal evaporation	~90 nm	600 nm	36.10 MS·m^{-1}	[13], [15]
Au	Pulsed laser deposition	500 nm	30 nm		[16]
Au	Sputtering	130 to 260 nm	60 to 70 nm	45.21 MS·m^{-1}	[15], [17]
Ag	Physical vapor deposition	75 nm	18 nm	0.29 MS·m^{-1}	[18]
C	Doctor blade	4.8 µm	50 to 100 nm	66.67 S·m^{-1}	[19], [20]

3. Methodology

3.1 Aluminium Thin Film Contact Layer Fabrication

The aluminium thin films were deposited onto a 2 cm by 2 cm glass substrate. The glass substrate is sonicated in soapy water, acetone, ethanol, and deionized water to clean it. Strips of 0.5 mm-diameter aluminium wires (0.5 mm-dia, annealed, Puratronic, 99.999%) are prepared with varying lengths (5 to 20 cm). Each of the wires is cleaned with isopropyl alcohol before being used. A YKY Compact DC Magnetron Sputtering and Thermal Evaporator is used for the thermal evaporation of the aluminium films. The source wire is balled up and placed into the tungsten wire boat in the vacuum chamber, then the glass substrates are masked with glass pieces to leave a 2 cm by 1 cm strip in the middle. Then they are mounted onto the substrate holder and placed over the boat containing the source material at a separation distance of 3 cm. The vacuum chamber is then sealed and left to pump down to 4 Pa over the course of 2 hrs. Once the pressure condition is met, the source current is slowly increased until the tungsten boat starts to glow bright orange at 32 A; here the aluminium wire evaporation starts. Once the film has formed, the current is held for a few more seconds before quickly decreasing all the way to zero. The set-up is left to cool for 30 mins before the samples are taken out. Four different aluminium (Al) thin film samples, A, B, C, and D, with varying film thickness, were obtained.

3.2 Aluminium Thin Film Measurements

The thickness of the samples was obtained by making a vertical step on the film. A MarSurf M 400C stylus profilometer was used to measure the thickness. The traversal length was set to 1.5 mm, and the cutoff length was set to 0.08 mm. Measurements were taken at four different points, and the average thickness was calculated. The electrical properties of the aluminium films of each sample were measured using a Keithley 236 Source Measure Unit (SMU) 4-point probe. The SMU was set to current-voltage (*I-V*) measurement, linear stair, with a start and stop voltage of -3 V to 3 V and a 0.1 V step. No delay was set, and the bias voltage is zero. Auto range was selected, and the settings were saved before starting the operation. The operation was made to sweep from the start to the stop voltage range, and each of the current values was recorded and tabulated. Nanosurf Easyscan atomic force microscopy (AFM) was used to obtain the surface morphology and particle size of the samples. The samples were measured over an area of 5 µm by 5 µm. The average particle sizes were taken by using the measure length function in the Nanosurf Easyscan 2 software. The root-mean-square (RMS) area roughness was obtained using the built-in area roughness calculation function.

4. Results and Discussions

4.1 Thickness of Aluminium Metal Contact Layer

In Fig. 1, the shiny, mirror-like appearance depicts the area of the aluminium (Al) thin film. The thickness of each sample (A, B, C, and D) is compiled in Table 2. The wire source lengths of 5 cm, 10 cm, 15 cm, and 20 cm yielded a thickness of 188 nm, 38 nm, 450 nm, and 69 nm, respectively, for samples A, B, C, and D. Sample D also depicted a sample thickness of 69 nm which is comparable to the results obtained by other work as illustrated in Table 1 [13].

The varying length of the Al wire source did not seem to have affected the thickness of the deposited film. Therefore, controlling the thickness of the deposited Al films by varying the length of the Al wire source is not a viable method and is unreliable. Normally, the thickness can be controlled more precisely using a thermal evaporation system that incorporates an in-situ thickness monitoring sensor and a shutter [21].

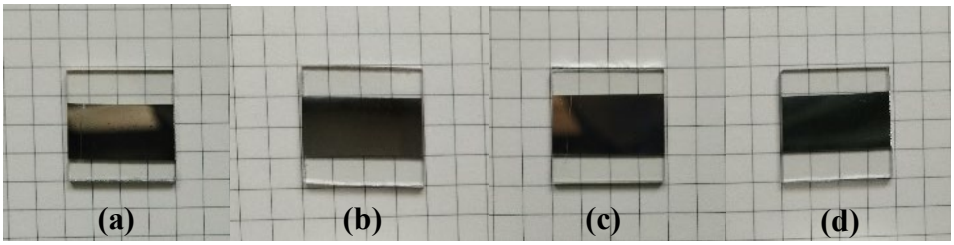

Fig. 1 *Images of the four aluminium thin film samples produced, samples (a) A, (b) B, (c) C, and (d) D using 5, 10, 15, and 20 cm of aluminium source wire*

Table 2 *Aluminium film thickness of samples A, B, C, and D*

Sample	Wire length (cm)	Thickness (nm)
A	5	188
B	10	38
C	15	450
D	20	69

4.2 Surface Morphology of Aluminium Metal Layer

The AFM images of the aluminium particles depicted in Fig. 2 are densely packed with round to oval-shaped particles distributed uniformly all over the film surface for all four samples. As can be seen in Table 2, Sample D showed the smallest average particle size of 45.24 nm, while Sample C had the largest average particle size of 149.44 nm. Sample D also exhibited the roughest surface topography at 5.98 nm, and Sample B was the smoothest out of all samples at 4.61 nm.

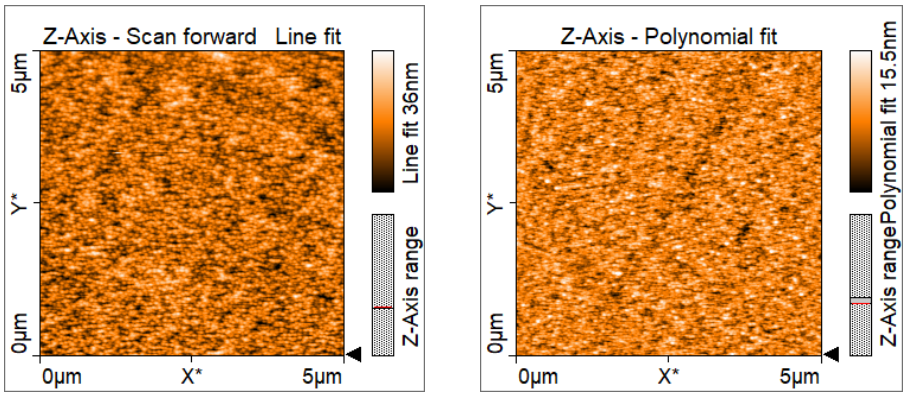

(a) **(b)**

Int. Journal of Integrated Engineering Vol. 16 No. 3 (2024) p. 28-35

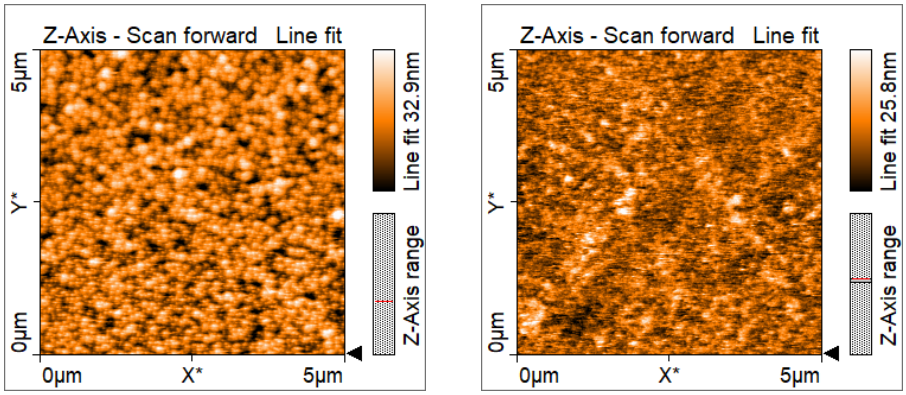

Fig. 2 *5 µm × 5 µm AFM images of aluminium thin film samples, (a)-(d) for samples A, B, C, and D*

Table 3 *Average particle size and root-mean-square (RMS) area roughness of the aluminium thin film samples*

Sample	Sample Thickness (nm)	Average Particle Size (nm)	RMS Area Roughness (nm)
A	188	93.64	5.20
B	38	74.79	4.61
C	450	149.44	5.85
D	69	45.24	5.98

From these results, the average particle size and area roughness seem to increase with increasing film thickness. Based on studies, the larger particle size correlates to a better electromigration resistance, and thin films can also improve the electromigration effect, which is an important mechanism for the dissipation of substantial amounts of power densities to prevent the melting of thin films [22], [23]. Based on a study by Quintana et al., grain size increases as the film thickness increases, and a larger grain size contributes to a more uniform film morphology [24]. The electrical resistivity of thin films is also affected by their morphology, in which an increase in the surface scattering of conduction electrons can contribute to the increase in resistivity [25]. As such, the results obtained in this study are comparable to the available literature.

4.3 Electrical Properties of Aluminium Metal Contact Layers

The *I-V* characteristics of the aluminium (Al) thin films were measured using a Keithley 236 SMU with a 4-point probe. The resistance (R) was calculated from the *I-V* values obtained. The sheet resistance (R_s) was calculated using the following equation:

$$R_s = R\left(\frac{\pi}{\ln 2}\right) \tag{1}$$

The resistivity (ρ) is then obtained from the sheet resistance (R_s) using the formula, where t is the film thickness and k = 0.9345 is the geometric correction factor of the 4-point probe. The data are then tabulated in Table 3.

$$\rho = R_s(t)(k) \tag{2}$$

The *I-V* characteristics of all samples show a linear graph in Fig. 3(a). With increasing thickness of the Al film, a decrease in resistance is illustrated, as seen in Fig. 3(b). Correspondingly, the sheet resistance also displays a decrease with increasing thickness (Fig. 3(c)). The resistivity of the films show a decrease as the thickness in increase at the lower thickness range (38 to 69 nm), in which is comparable to literature [26]. Conversely, at the higher thickness range of 188 to 450 nm, the resistivity of the films is shown to increase with increasing thickness (Fig. 3(d)). As can be observed from the curves, the electrical properties of the thinner Al films, 38 nm and 69 nm, differ greatly from those of the thicker film, 188 nm and 450 nm. This is evident as the resistance, sheet resistivity, and resistivity of thin films differ from their bulk counterparts as they are governed by many factors, including their thickness, rate of deposition, temperature, grain boundaries of the particles, and also the quantum confinement effect [27], [28]. Based on this study, Sample D with a thickness of 69 nm has demonstrated the

lowest resistivity of 2.31 μΩ·m and the highest conductivity value of 432.90 kS·m^{-1}, as conductivity is the inverse of resistivity. Sample C, on the other hand, demonstrated the highest resistivity recorded at 10.85 μΩ·m with a conductivity of 92.17 kS·m^{-1}. Samples A and B presented resistivities of 6.14 and 3.36 μΩ·m and conductivities of 162.86 and 297.62 kS·m^{-1}, respectively. Samples A, B, and D show promising applications as the metal contact layer for the device due to their higher conductivity values. Contrarily, none of the samples show a conductivity that is comparable to the literature that was presented in Table 1, which illustrated a conductivity of 36.10 MS·m^{-1}, which is a resistivity of 27.70 nΩ·m.

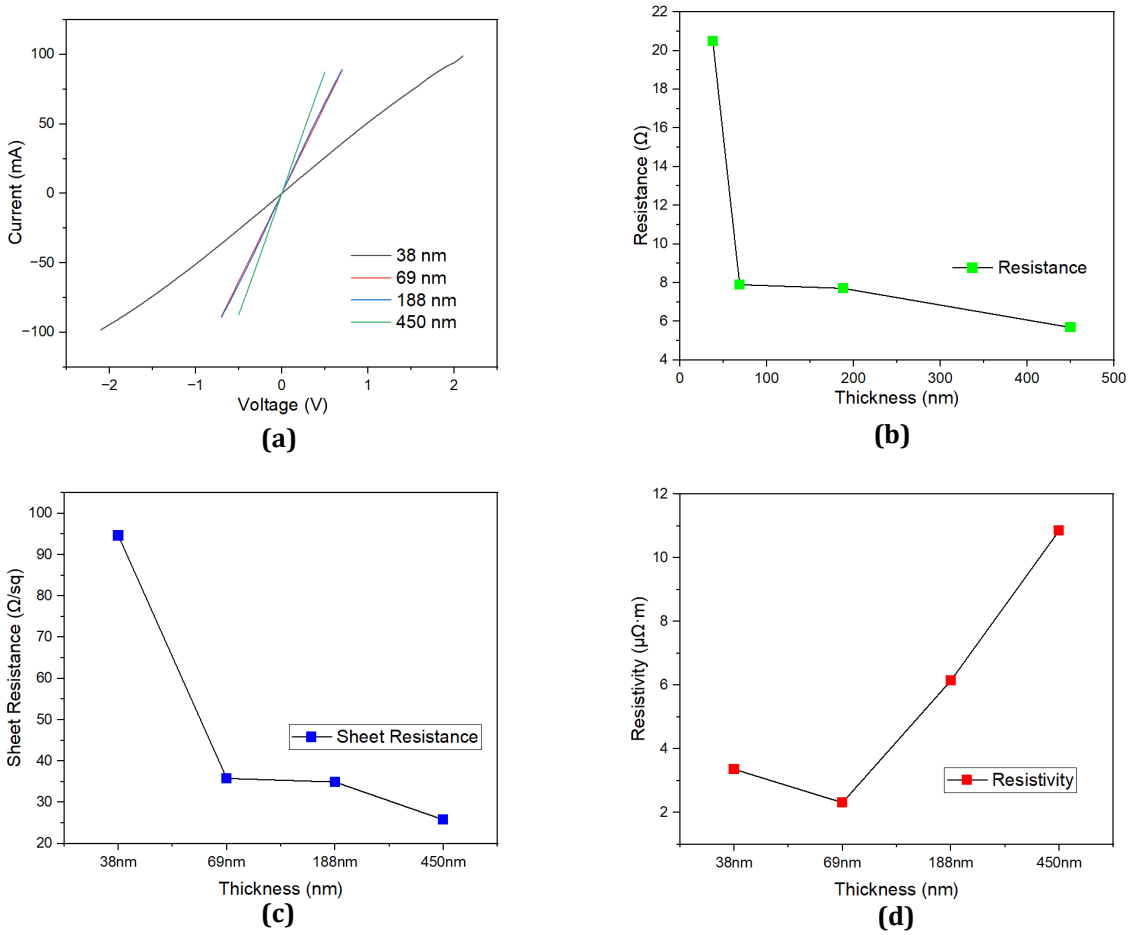

Fig. 3 *(a) I-V characteristics; (b) resistance; (c) sheet resistance; and (d) resistivity curves for the aluminium thin film samples*

Table 4 *Electrical properties of the aluminium thin film samples*

Sample	Thickness (nm)	Resistance (Ω)	Sheet Resistance (Ω/sq)	Resistivity (μΩ·m)
A	188	7.71	34.94	6.14
B	38	20.88	94.64	3.36
C	450	5.69	25.79	10.85
D	69	7.90	35.81	2.31

5. Conclusions

In this paper, the electrical properties of aluminium thin films in correlation to the thickness and morphology of the films are investigated. Based on the findings, Sample A was found to be most suitable for the application as the metal contact layer for the perovskite solar cell. This is due to the good demonstration of resistivity and conductivity (6.14 μΩ·m, 162.86 kS·m^{-1}), as well as adequate thickness, particle size, and roughness. This sample was decided upon due to the balance needed between higher conductivity and large particle size to ensure better charge transportation of the aluminium film. Although the Sample D showed the highest conductivity of 432.90 kS·m^{-1}, the AFM results showed the highest RMS area roughness of 5.98 nm. This shows that the film formed in

Sample D is not smooth and has many holes which can affect the overall performance of the film, as such this sample was not chosen.

Acknowledgement

The research was funded by the Ministry of Higher Education (MOHE), Malaysia, under the Fundamental Research Grant Scheme (FRGS 2022-1) (Project Ref: FRGS/1/2022/TK08/MMU/03/1).

Conflict of Interest

Authors declare that there is no conflict of interests regarding the publication of the paper.

Author Contribution

The authors confirm contribution to the paper as follows: ***study conception and design:*** *Pei-Ling Low, Kah-Yoong Chan;* ***data collection:*** *Rachael Wan Lyn Sia;* ***analysis and interpretation of results:*** *Rachael Wan Lyn Sia, Pei-Ling Low, Abdelrahman Hamed Ebrahem Abdelhamed, Gregory Soon How Thien, Yew-Keong Sin, Kah-Yoong Chan;* ***draft manuscript preparation:*** *Rachael Wan Lyn Sia. All authors reviewed the results and approved the final version of the manuscript*.

References

[1] Shi, Z. and Jayatissa, A. (2018). Perovskites-Based Solar Cells: A Review of Recent Progress, Materials and Processing Methods. *Materials*, 11(5), p.729. https://doi.org/10.3390/ma11050729.

[2] Baikie, T., Fang, Y., Kadro, J.M., Schreyer, M., Wei, F., Mhaisalkar, S.G., Graetzel, M. and White, T.J. (2013). Synthesis and crystal chemistry of the hybrid perovskite (CH3NH3)PbI3 for solid-state sensitised solar cell applications. *Journal of Materials Chemistry A*, 1(18), p.5628. https://doi.org/10.1039/c3ta10518k.

[3] Mishra, A.K. and Shukla, R.K. (2020). Fabrication and characterization of perovskite (CH3NH3PbI3) solar cells. *SN Applied Sciences*, 2(3). https://doi.org/10.1007/s42452-020-2054-3.

[4] Razza, S., Castro-Hermosa, S., Di Carlo, A. and Brown, T.M. (2016). Research Update: Large-area deposition, coating, printing, and processing techniques for the upscaling of perovskite solar cell technology. *APL Materials*, 4(9), p.091508. https://doi.org/10.1063/1.4962478.

[5] Younas, M., Gondal, M.A. and Dastageer, M.A. (2020). Fabrication of perovskite solar cells using novel 2D / 3D -blended perovskite single crystals. *International Journal of Energy Research*, 45(4), pp.5555–5566. https://doi.org/10.1002/er.6183.

[6] Ma, X., Peyton, A. and Zhao, Y. (2005). Measurement of the electrical conductivity of open-celled aluminium foam using non-contact eddy current techniques. *NDT and E International*, 38(5), pp.359–367. https://doi.org/10.1016/j.ndteint.2004.10.003.

[7] Sahoo, S.K., Manoharan, B. and Sivakumar, N. (2018). Introduction: Why Perovskite and perovskite solar cells? *Perovskite Photovoltaics*, pp.1–24. https://doi.org/10.1016/b978-0-12-812915-9.00001-0.

[8] Poespawati, N.R., Dzikri, I., Sulistianto, J., Abuzairi, T., Hariadi, M. and Purnamaningsih, R.W. (2018). Perovskite Solar Cells Based on Organic-metal halide Perovskite Materials. *2018 4th International Conference on Nano Electronics Research and Education (ICNERE)*. https://doi.org/10.1109/icnere.2018.8642587.

[9] Lin, L., Jiang, L., Li, P., Qiu, Y. and Yan, Q. (2019). Numerical analysis of inverted-structure perovskite solar cell based on all-inorganic charge transport layers. *Journal of Photonics for Energy*, 9(02), p.1. https://doi.org/10.1117/1.jpe.9.024501.

[10] [Gonzalez-Pedro, V., Juarez-Perez, E.J., Arsyad, W.-S., Barea, E.M., Fabregat-Santiago, F., Mora-Sero, I. and Bisquert, J. (2014). General Working Principles of CH3NH3PbX3Perovskite Solar Cells. *Nano Letters*, 14(2), pp.888–893. https://doi.org/10.1021/nl404252e.

[11] Qiu, C., Wu, Y., Song, J., Wang, W. and Li, Z. (2022). Efficient Planar Perovskite Solar Cells with ZnO Electron Transport Layer. *Coatings*, 12(12), pp.1981–1981. https://doi.org/10.3390/coatings12121981.

[12] Hossain, M.F., Naka, S. and Okada, H. (2018). Fabrication of perovskite solar cells with ZnO nanostructures prepared on seedless ITO substrate. *Journal of Materials Science: Materials in Electronics*, 29(16), pp.13864–13871. https://doi.org/10.1007/s10854-018-9518-x.

[13] Nouri, E., Mohammadi, M.R. and Lianos, P. (2017). Inverted perovskite solar cells based on lithium-functionalized graphene oxide as an electron-transporting layer. *Chemical Communications*, 53(10), pp.1630–1633. https://doi.org/10.1039/c6cc09876b.

[14] Chandu V. V. Muralee Gopi, Mallineni Venkata-Haritha and Kandasamy Prabakar (2017). Low-temperature easy-processed carbon nanotube contact for high-performance metal- and hole-transporting layer-free perovskite solar cells. *Journal of Photochemistry and Photobiology A: Chemistry*, 332, pp.265–272. https://doi.org/10.1016/j.jphotochem.2016.09.003.

[15] De Vries, J.W.C. (1988). Temperature and thickness dependence of the resistivity of thin polycrystalline aluminium, cobalt, nickel, palladium, silver and gold films. *Thin Solid Films*, 167(1-2), pp.25–32. https://doi.org/10.1016/0040-6090(88)90478-6.
[16] N.N. Nedyalkov, Nikolov, A., P.A. Atanasov, Alexandrov, M., Mitsuhiro Terakawa and Shimizu, H. (2014). Nanostructured Au film produced by pulsed laser deposition in air at atmospheric pressure. *Optics and Laser Technology*, 64, pp.41–45. https://doi.org/10.1016/j.optlastec.2014.03.022.
[17] Vitrey, A., Álvarez, R., Palmero, A., María Ujué González and José Miguel García-Martín (2017). Fabrication of black-gold coatings by glancing angle deposition with sputtering. *Beilstein Journal of Nanotechnology*, 8, pp.434–439. https://doi.org/10.3762/bjnano.8.46.
[18] Ding, G., Clavero, C., Schweigert, D. and Minh Tung Le (2015). Thickness and microstructure effects in the optical and electrical properties of silver thin films. *AIP Advances*, 5(11), pp.117234–117234. https://doi.org/10.1063/1.4936637.
[19] Wu, C.-S., Chang, T.-W., Teng, H. and Lee, Y.-L. (2016). High performance carbon black counter electrodes for dye-sensitized solar cells. *Energy*, 115, pp.513–518. https://doi.org/10.1016/j.energy.2016.09.052.
[20] Wu, Z., Chen, Z., Logan, J.M., Sippel, J., Nikolou, M., Kamaras, K., Reynolds, J., Tanner, D.B., Hebard, A.F. and Rinzler, A.G. (2004). Transparent, Conductive Carbon Nanotube Films. *Science*, 305(5688), pp.1273–1276. https://doi.org/10.1126/science.1101243.
[21] Pan, C.A. and Ma, T.P. (1980). High-quality transparent conductive indium oxide films prepared by thermal evaporation. *Applied Physics Letters*, 37(2), pp.163–165. https://doi.org/10.1063/1.91809.
[22] Pierce, D.G. and P.G. Brusius (1997). Electromigration: A review. *Microelectronics Reliability*, 37(7), pp.1053–1072. https://doi.org/10.1016/s0026-2714(96)00268-5.
[23] Vaidya, S. and Sinha, A.K. (1981). Effect of texture and grain structure on electromigration in Al-0.5%Cu thin films. 75(3), pp.253–259. https://doi.org/10.1016/0040-6090(81)90404-1.
[24] Quintana, P., Oliva, A.I., Ceh, O., Corona, J.E. and Aguilar, M. (1999). Thickness effects on aluminum thin films. *Superficies y vacío*, [online] (9), pp.280–282. Available at: http://www.redalyc.org/articulo.oa?id=94200973 [Accessed 26 Oct. 2023].
[25] Kim, H.C., Alford, T.L. and Allee, D.R. (2002). Thickness dependence on the thermal stability of silver thin films. *Applied Physics Letters*, 81(22), pp.4287–4289. https://doi.org/10.1063/1.1525070.
[26] Lacy, F. (2011). Developing a Theoretical Relationship between Electrical resistivity, temperature, and Film Thickness for Conductors. *Nanoscale Research Letters*, 6(1). https://doi.org/10.1186/1556-276x-6-636.
[27] Avilés, F., Ceh, O. and Oliva, A. (2005). PHYSICAL PROPERTIES OF AU AND AL THIN FILMS MEASURED BY RESISTIVE HEATING. *Surface Review and Letters*, 12(01), pp.101–106. https://doi.org/10.1142/s0218625x05006834.
[28] Ludmila Eckertová (1977). *Physics of Thin Films*. Springer US. https://doi.org/10.1007/978-1-4615-7589-4.